atmosphere

MDPI

Review

NLOS Communication: Theory and Experiments in the Atmosphere and Underwater

Vladimir V. Belov [1,*], Irit Juwiler [2], Nathan Blaunstein [2], Mikhail V. Tarasenkov [1] and Egor S. Poznakharev [1]

[1] V.E. Zuev Institute of Atmospheric Optics of the Siberian Branch of the Russian Academy of Science, Academician Zuev Sq., 1, Tomsk 634055, Russia; tmv@iao.ru (M.V.T.); 724_pes1992@iao.ru (E.S.P.)
[2] Center for E.O, Development of LASER Technologies and their Applications, Shamoon College of Engineering, Ashdod 77245, Israel; iritj@sce.ac.il (I.J.); nathan.blaunstein@hotmail.com (N.B.)
* Correspondence: belov@iao.ru; Tel.: +8-3822-492-237

Received: 16 September 2020; Accepted: 16 October 2020; Published: 19 October 2020

Abstract: In this paper, we present investigations of non-line-of-sight (NLOS) communication carried out in Russia and in collaboration with researchers in Israel. The theories of radiative transfer and linear systems provide the theoretical basis for this joint research, and experimental results demonstrate that maximal ranges for NLOS communication through atmospheric channels can reach hundreds of kilometers in the visible range and tens of kilometers in the ultraviolet (UV) range of the spectrum. Finally, we predict the range of bistatic underwater communication systems can reach hundreds of meters.

Keywords: non-line-of-sight optical communication; extinction; scattering; Signal Propagation; radiation transfer equation; Monte Carlo method; visual and ultraviolet band

1. Introduction

The exact date when optical ranging was first used for high-speed messaging is, of course, unknown, but it can be assumed that it began many centuries ago when signal smoke, torches, etc. were used for communication over long distances. Now, this type of communication continues to be used for messaging using the Morse alphabet and searchlights equipped with light shutters. However, these technologies of optical communication have long been replaced by new methods based on laser radiation and optical fiber for secure communication channels. In particular, these have culminated in the development of the global Internet. These new technologies prompt the question of whether there is any merit in the development of atmospheric and underwater optical communication systems with open communication channels? Radio communication through the atmosphere has a long history, it operates in all weather, and is available practically everywhere, whereas through water media, acoustic communication systems with open channels are widely used.

However, there are conditions under which there is value in developing and using optoelectronic atmospheric or underwater optical communication systems. i.e., when radio communication is impossible or undesirable, or when the rate of information transfer underwater by acoustic communication systems is insufficient. This explains the need for the development of atmospheric or underwater optical communication systems with open channels for information exchange, when the receiver and source locations are distanced but their optical axes lie in one plane. Optoelectronic systems (OES) of this type are called line-of-sight (LOS) systems. Non-scattered optical radiation comprises the useful signal in LOS systems. Many theoretical and experimental investigations of these systems have been published and continue to be published extensively (for example, see [1]).

In the present work, results of investigations of optoelectronic communication systems (OECS) in which the useful signal is comprised of scattered or reflected optical radiation are considered. These OECS are called non-line-of-sight (NLOS) systems, and in Russia they are more often called over-the-horizon or bistatic systems (for example, see [2–12]). If communication is based on reflected radiation (from a plane, a building, a ship hull, a submarine surface, etc.), this communication type is called direct NLOS. For LOS optical communication, high rates of information transfer are common. However, unavoidable interruptions of communication caused by opaque screens occluding the receiver field-of-view, or by beam wandering over the input pupil of the receiver due to the atmospheric (or water) turbulence, may occur. NLOS communication has none of these disadvantages and, in addition, it is multi-address (broadcast). In the present review, we focus on theoretical and experimental investigations of NLOS communication systems performed by Russian researchers. These works were initially conducted at the Institute of Laser Physics of the SB RAS under the supervision of Professor B. V. Poller in 2004 [2], and were performed only on atmospheric paths. Over the past 7 years, investigations on problems of NLOS communication in atmospheric and water media have been carried out in the Russian Federation only at the Institute of Atmospheric Optics of the Siberian Branch of the Russian Academy of Science (SB RAS). Some aspects of joint research work, regarding optical waves and laser beams in the irregular atmosphere performed with our co-authors from Israel, were published by *IEEE* in 1970 [3] and by CRC Press in 2018 [4], and in papers [12]. The present paper summarizes the main results of this research undertaken during the past decade.

2. Research Objectives and Statement of Problems

Any bistatic OECS can be described by a set of the following input parameters: laser radiation wavelength λ, angular beam divergence ν_s, beam radius r_s, orientation of the beam optical axis $\boldsymbol{\omega}_s$ (θ_s, φ_s), average source power P_s, receiver field-of-view angle ν_d, input pupil radius r_d, orientation of the receiver optical axis $\boldsymbol{\omega}_d$ (θ_d, φ_d), spectral photodetector sensitivity $S(\lambda)$, and noise level P_f. The most important external parameter of the bistatic OECS is the base length L_d (the distance between the source and the receiver). A block diagram of a typical NLOS communication system is shown in Figure 1. From our point of view, any NLOS system will have these blocks (Figure 1), where blocks "Telescope", "Photodetector", and "Signal demodulator" are related to the detector of optical waves, and blocks "Signal modulator", "Laser", and "Optics" are related to the source of radiation. Characteristics of these blocks comprise a real optical-electronic bistatic system.

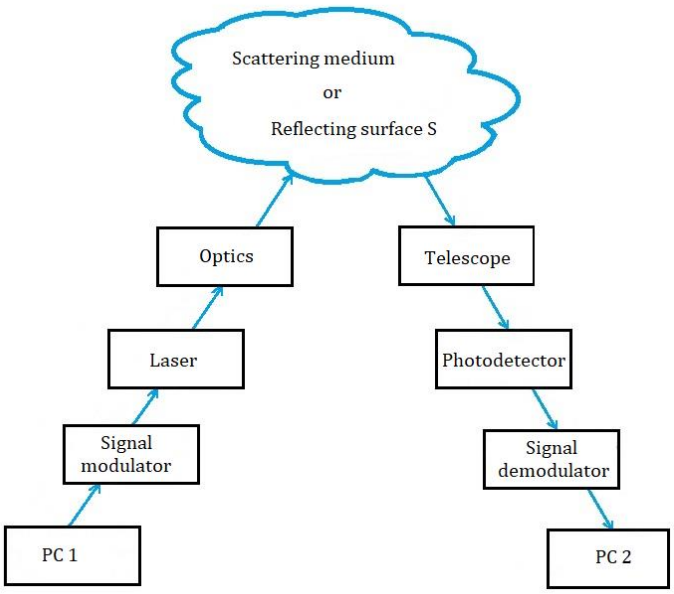

Figure 1. General block diagram of the non-line-of-sight (NLOS) communication system.

We also should note that we do not highlight the ice, because ice has both reflection and scattering properties of optical radiation. These properties are listed in Figure 1. If we choose to highlight ice, then for atmospheric systems or for experiments underwater during the summer, this drawing will not be suitable and another drawing would be necessary. Under "scattering medium or reflecting surface *S*" we define the atmosphere or water region, including that covered by ice, which scatters optical waves by medium or reflects waves from surfaces of flying or moving vehicles, such aircraft. The functions of the units shown in Figure 1 are as follows. The control computer (PC 1, see Figure 1) provides information (texts, images, video series, control commands, etc.) to be transmitted through the communication channel. The information modulates laser radiation in the "Signal modulator" unit. After creating the output characteristics in the "Optics" unit, laser radiation is transmitted to the open communication channel. The radiation that has been scattered in the atmosphere or underwater is then focused with a telescope onto the input pupil of a photodetector and is fed to the "Signal demodulator" unit, where received signals are decoded and the retrieved information reaches the computer (PC 2). In the "Optics" unit, the radiation wavelength λ_1 can be converted to λ_2 using, for example, nonlinear crystals. Sometimes, converting the visible range of radiation into UV can be more economical than the purchase of a UV laser with a given pulse repetition rate. The ability exists to modulate and demodulate the radiation in the visible and UV ranges using the same optoelectronic units. We emphasize that the UV radiation used in the experiments was not dangerous for the operators because only scattered radiation is detected, and the laser beam is thus directed into the upper hemisphere relative to the Earth's surface. Figure 2 shows a coplanar configuration of a bistatic communication channel.

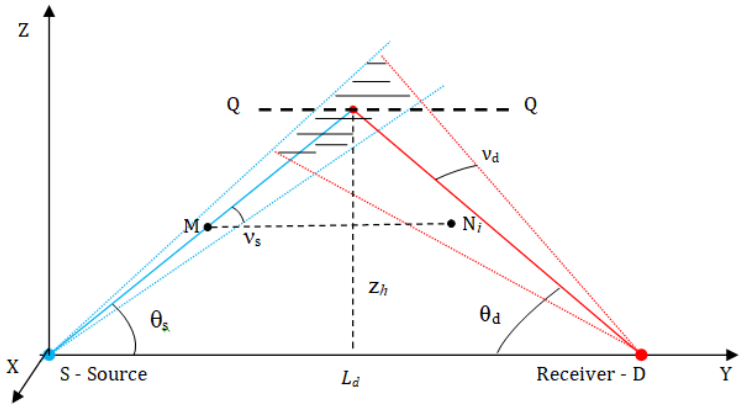

Figure 2. Geometric scheme of channels of bistatic coplanar communication.

The main OECS output characteristics are the error probability *p*, its standard deviation (SD) σ, and the rate of symbol transfer. Each of these characteristics depends on the above-listed parameters of the transceiving system and on the geometric schemes of the bistatic OECS channels. Therefore, the main objectives of theoretical and experimental investigations of bistatic communication or control systems are the determination of the values of these characteristics, and their dependence on all of the other parameters of a particular OECS and its units, in addition to the optical state of the radiation propagation channels from the source to the receiver (for example, see [2–26] and the bibliography therein). In addition, the goal of experimental investigations is to confirm (or refute) theoretical predictions regarding the feasibility of a specific OECS design and its particular characteristics.

3. Theoretical Background

From a system analysis viewpoint, any OECS described by Figure 1 has two parts: the transceiver (transmitter-receiver) system and the external communication channel. For given optoelectronic units, the output characteristics of the OECS shown in Figure 2 will depend on the optical state of the radiation propagation channel from the source to the receiver. The state of the atmosphere or water

can change between far-apart limits [27–31]. Hence, in [2–26] much attention was focused on an analysis of the influence of the input OECS parameters and the optical properties of the atmosphere on the communication quality. The optical properties of the communication channel, with all other conditions remaining the same, could limit the maximum transmission range of an OECS and increase the error probability. One way to overcome these difficulties is to apply a controllable decrease in the rate of information transfer. The transfer properties of bistatic OECS channels were investigated in the context of the theory of short-wavelength radiation transfer in scattering and absorbing media (e.g., the atmosphere and water) and the theory of linear system analysis. The radiation transfer equation (RTE) establishes a relationship between the light flux intensity at a given point, and in a preset direction in the medium and its optical characteristics. In the integral-differential form, it can be written as

$$\frac{1}{c}\frac{\partial I}{\partial t} + (\boldsymbol{\omega}, grad\, I) = -\beta_{ext} I + \beta_{sc}\int_{\Omega} I\left(\mathbf{r}, \boldsymbol{\omega}'\right) g\left(\mathbf{r}, \boldsymbol{\omega}, \boldsymbol{\omega}'\right) d\boldsymbol{\omega}' + \Phi_0(\mathbf{r}, \boldsymbol{\omega}), \tag{1}$$

where $I = I\,(\lambda,\mathbf{r},\boldsymbol{\omega})$ is the light intensity at a point $\boldsymbol{r}$ in direction $\boldsymbol{\omega}$, c is the velocity of light, $\beta_{ext}(\lambda,\mathbf{r})$ is the extinction coefficient at the point $\mathbf{r}$, $\beta_{sc}(\lambda,\mathbf{r})$ is the scattering coefficient at the point $\mathbf{r}$, $g\ (\lambda,\mathbf{r},\boldsymbol{\omega},\boldsymbol{\omega}')$ is the normalized scattering phase function at the point $\mathbf{r}$ in the direction $\boldsymbol{\omega}$, $\boldsymbol{\omega}'$ is the direction of radiation propagation before scattering, and Φ_0 is the source function at the point $\mathbf{r}$ in the direction $\boldsymbol{\omega}$. Equation (1) is linear with light intensity; therefore, it is expedient to analyze the transfer properties of the bistatic communication channel in the context of linear systems theory, that is, to investigate the channel response $h(t)$ to the input $\delta(t)$ pulse depending on the input OECS parameters.

Equation (1) has no general analytical solution. To solve it for NLOS communication systems, various algorithms using the Monte Carlo method (from direct simulation algorithms [18] to algorithms based on modified double local estimates [9]) are often used. In [9] we suggested a modified algorithm of the Monte Carlo method with double local estimates from each point of photon collision in the medium with scattering centers at each preset time interval. The procedure of estimation involves the following steps [9].

A mobile Cartesian coordinate system centered at the receiver point D is constructed at each collision point. The Dy' axis is directed toward the point of next collision M, the Dz' axis is perpendicular to the Dy' axes and lies in the plane containing the source axis and the vertical, and the Dx' axis is perpendicular to the Dy' and Dz' axes and oriented such that the three vectors form a right-handed system of coordinates. A random direction (a, b, c) uniformly distributed over the solid angle is chosen within the field-of-view of the receiving system in the mobile system of coordinates.

In the mobile system of coordinates, sub-regions are constructed within the field-of-view of the receiving system. The boundaries of these sub-regions are formed by the field-of-view cones and ellipsoids of rotation. The equations of the ellipsoids of rotations are defined by the focal parameters P_i and eccentricities e_i. The corresponding expressions were presented in [9]. For each sub-region thus obtained, its own intermediate collision point N_i is constructed on the beam formed by the direction (a, b, c). For each intermediate collision point N_i, the double local estimate of the radiation intensity is constructed after scattering at point M and arrival at point N_i, and then further scattered at this point and arriving at the receiving system D. The estimate is calculated from the formula:

$$\begin{aligned} I_{i,j,k} = {} & \omega_k \cdot 2\pi\left(1 - \cos\tfrac{\nu_d}{2}\right)\cdot\left(\tfrac{P_i}{1-e_i b} - \tfrac{P_{i-1}}{1-e_{i-1} b}\right)\cdot\frac{\sigma_s\left(\vec{r}_M\right) g\left(\vec{r}_M, \cos\gamma_{1,i}\right)}{2\pi\sigma_t\left(\vec{r}_M\right) r^2_{MN_i}}\times \\ & \times\frac{\sigma_s\left(\vec{r}_{N_i}\right) g\left(\vec{r}_{N_i}, \cos\gamma_{2,i}\right)}{2\pi}\exp\left(-\tau_{MN_i}\right)\exp\left(-\tau_{N_i D}\right) \end{aligned} \tag{2}$$

where ω is the photon "weight" at the collision point M, σ_s is the scattering coefficient, σ_t is the extinction coefficient, g is the scattering phase function, r_M is the radius vector of the collision point M, r_{N_i} is the radius-vector of the intermediate point of collision N_i, $\gamma_{1,i}$ is the angle of scattering measured from the direction of the photon trajectory before the collision to the MN_i direction, $\gamma_{2,i}$ is the angle of scattering from the direction MN_i to the direction N_iD, b is the second coordinate of the random

direction (a, b, c) in the mobile system of coordinates, τ_{MN_i} is the optical thickness from the collision point M to the intermediate collision point N_i, and τ_{N_iD} is the optical thickness from the intermediate collision point to the receiving system. In [9] the unbiased nature of the estimates obtained using this algorithm was proven. It was also shown that this algorithm is much less energy-consuming than the conventional algorithm of the double local estimate.

Clearly, the single-scattering approximation for estimating the impulse response characteristic $h(t)$, pulse broadening, etc., has limitations. This follows from the analysis of the impulse responses of NLOS communication channels, whose typical form is shown in Figure 3. The time interval $[t_1, t_2]$ shown in Figure 3 indicates the period of intersection of the laser beam divergence angle with the field-of-view angle of the receiving system (forming the hatched area shown in Figure 2). The function $h(t)$ for t beyond this interval is determined by radiation that has been multiply scattered, that is, the leading and trailing fronts of the impulse response $h(t)$ shown in Figure 3 can be determined by solving the RTE (1) allowing for multiple scattering of no less than the second order. For atmospheric OECS, it is possible to choose the spectral characteristics of laser sources over a wide range of the spectrum, from UV to IR. In water, this choice is limited to the visible (green or dark blue) range of the spectrum because of the strong absorption by water of non-visible radiation (for example, see [12,26]).

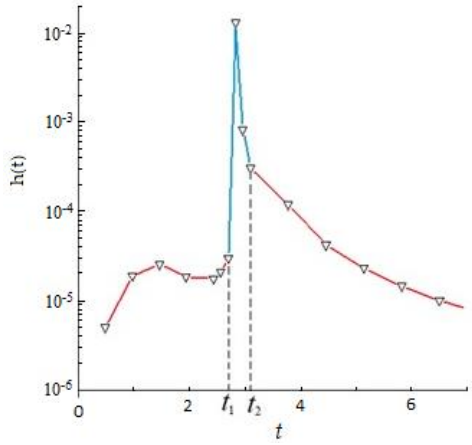

Figure 3. Example of the impulse response simulated by the Monte Carlo method.

There are a number of drawbacks of the bistatic communication configuration that could result in its unfeasibility. Clearly, for successful communication, the power of the received information-bearing signal must exceed the intrinsic photodetector noise power P_f. Communication errors arise when this condition is occasionally violated. This can be caused by turbulence in the optical characteristics of the communication channel or by local clots of optically dense scattering or absorbing formations (fragments of smoke plumes, cloudy media, etc.) intersecting the receiver field-of-view. Communication may be unfeasible even when the information-bearing signal power exceeds the noise power. This may be observed when values of the impulse response at $t < t_1$ and $t \to t_1$ or at $t > t_2$ and $t \to t_2$ become close or equal to max $h(t)$ in the central part (see Figure 3). Proceeding from these general considerations of the optical radiation's interaction with scattering and absorbing media, we now consider the influence of some optical and geometric parameters of bistatic OECS on the communication range and error probability. Consider the following: fix all geometric and optical parameters and all photodetector characteristics; let the divergence angle ν_s of the laser radiation beam be zero and the communication range be L_d. It is clear from Figure 2 that the maximum reasonable value is vs. $= \theta_s$ rather than $\pi/2$. To obtain the L_d dependence on ν_s we increase it from zero to θ_s and examine the effect on the impulse response (Figure 3). The duration of its leading edge will decrease, that is, the interval $[0, t_1] \to 0$. The interval $[t_1, t_2]$ will monotonically increase, and the maximum value of the impulse response will decrease, thereby increasing the error probabilities and decreasing the maximum base distances L_d.

Now, we let all optical and geometric parameters of the OECS scheme (Figure 2) be fixed except for the field-of-view angle ν_d of the receiving optical system that will monotonically increase from zero. Assume that at $\nu_d = 0$ the communication range of the OECS is equal to L_d. It can be easily demonstrated that as ν_d, increases, the power at the leading edge of the impulse response $h(t)$ will increase, together with the time interval $[t_1, t_2]$ (Figure 3), but the maximal $h(t)$ will not increase. Both of these factors increase the communication errors, that is, from a certain critical ν_d value, the base L_d will decrease. It is straightforward to predict the dependence of L_d on some optical properties of the medium forming the OECS channel shown in Figure 2. Let the optical characteristics of the medium be homogeneous. Fix values of all other OECS parameters and let the medium be non-scattering. Obviously, when the base $L_d = 0$, the error probability $p = 0$, and the rate of symbol transfer $s = 0$. Now, let the scattering coefficient $\beta_{sc} \to \infty$; then, obviously, as $L_d \to 0$, the error probability $p \to 0$, and the rate of symbol transfer $s \to 0$. Hence, for each β_{sc} value there exists nonzero values of L_d, p, and s. This implies that for each set of input OECS parameters, there exists an optical state of the medium at which a maximal base distance L_d can be observed. This suggests that the optimal communication conditions (at least, from the viewpoint of the level of max $h(t)$) pertaining to variations in the orientation angles of the transmitted, θ_s, and receiving, θ_d, axes (given that all other OECS parameters remain the same) are realized when θ_s and $\theta_d \to 0°$. It is obvious that an increase in the average or peak laser radiation power will lead to an increase in the maximal L_d value.

In [7,9,20] results of statistical simulation of the impulse responses of the atmospheric and underwater communication channels using the Monte Carlo method, for various external and internal characteristics and parameters of the communication channels obtained in Russia at the Institute of Atmospheric Optics of the SB RAS (IAO SB RAS), were analyzed. A series of numerical experiments, discussed in [9], were performed with the LOWTRAN-7 optical aerosol-gas models of the atmosphere and the meteorological visibility ranges $S_M = 10$ and 50 km; wavelengths $\lambda = 0.3$, 0.5, and 0.9 μm; angles $\theta_s = \theta_d = 5°$; $\nu_s = 0.0034°$; $\nu_d = 2°$; and $L_d = 0.5$–200 km. In calculations, 30 packages, comprising 10^8 photon histories each, were simulated, and provided errors of estimating the response $h(t)$ not exceeding 0.15–10%. The main conclusions from the analysis of the transfer properties of the atmospheric communication channels performed in [9] are the following. For short base distances (2–3 km), with other conditions remaining unchanged, the received information-bearing pulse power was maximal at the radiation wavelength $\lambda = 0.3$ μm. For longer base distances and low turbidity of the media (meteorological visibility range $S_M \geq 50$ km), maximal power was reached at $\lambda = 0.5$ μm. For high atmospheric turbidity ($S_M \leq 10$ km), the maximal ranges were observed at $\lambda = 0.5$ μm and $\lambda = 0.9$ μm, depending on the orientation of the receiving plane. It was demonstrated that the maximal pulse transmission frequencies for bistatic optoelectronic communication systems were between 4×10^3 and 2×10^7 Hz, depending on the optical conditions in the atmosphere and geometric parameters of the communication channels.

In [20], in which underwater NLOS was studied, it was demonstrated that for communication at the wavelength $\lambda = 0.5$ μm and visibility depth $z_w = 30$ m for ranges 10–100 m and a wide variety of orientations of the source and receiver optical axes, the lower limit of radiation power recorded at the receiver must differ from the power of the radiation source by $\eta \geq 150$ dB. In this case, the maximum number of transmitted pulses $v_{\max}$ was between 3×10^6 Hz and 2×10^7 Hz for a source pulse duration of $\Delta t = 30$ ns. The transfer properties of underwater optical communication channels with scattered laser radiation were simulated for optical water characteristics taken from [29,31]. These simple discussions allow us to evaluate and estimate the coincidence between the obtained theoretical and experimental results. Here we want to note that during the above theoretical analysis, we did not account for the influence of atmospheric characteristics or water medium, or the characteristics of the detector or source on the probability of error in communication, because in Section 4, we proposed and realized techniques to control it at a real-time scale.

4. Experimental Investigations

Some examples of experimental investigations of the transfer characteristics of atmospheric bistatic channels can be found in [2,15–19]. In most publications, UV radiation sources with short transmission distances L_d were considered, and both lasers (including solid-state) and light-emitting diodes were used as pulsed radiation sources. In experiments with optical communication systems carried out at the IAO SB RAS, the following procedure for estimating the average communication errors μ and their standard deviations (SDs) σ in real time were used. The initial test image of a harmonic signal was formed (Figure 4a) and modulated the laser beam. The ordinate amplitudes of the transmitted periodic signal and the received signal are plotted on the ordinate axes in Figure 4. In other words, on the vertical axis in Figure 4 are depicted relative amplitudes of the transmitting and receiving periodical signal. In Figure 4, for both signals, input (a) and output (b) the values of the amplitude of the signal (along the ordinate axis) are in relative units and time (on the abscissa axis) is in relative units to time in free space conditions, that is, maximum of relative amplitude equals 250 ± 10 relative units, and minimum is equal to zero.

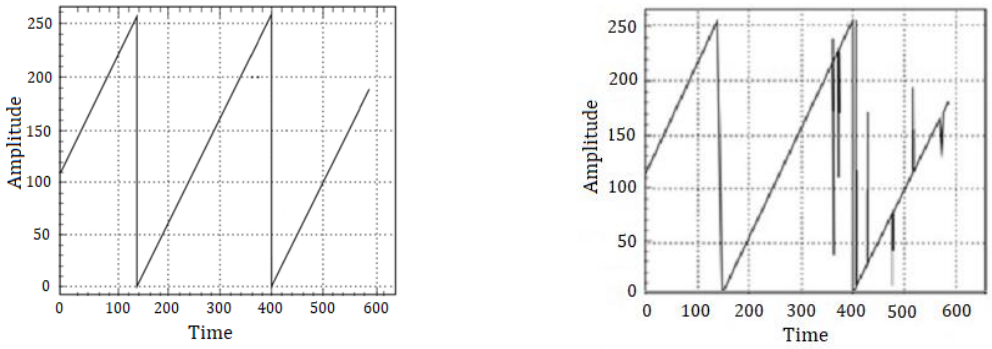

Figure 4. (**a**) Initial test signal; (**b**) received test signal image.

Let Z_i be the test signal amplitude at the i-th time moment and z_i be the received signal amplitude (Figure 4b). We consider that:

$$x_i = \left\{ \begin{array}{ll} 0 & if\ Z_i = z_i \\ 1 & if\ Z_i \neq z_i \end{array} \right\}, \tag{3}$$

Let N symbols be transmitted during the communication session, where $N = \sum_{j=1}^{m} n_j$, that is, the received series of symbols was subdivided into m packages, each having n_j symbols. We consider that the average number of erroneous received symbols, that is:

$$y_j = \frac{1}{n_j} \sum_{i=1}^{n_j} x_i, \tag{4}$$

is a random value. Then the average error probability for information transferred through the channel during the communication session is defined as:

$$\mu = \frac{1}{m} \sum_{j=1}^{m} y_j, \tag{5}$$

and its SD is:

$$\sigma = \sqrt{\frac{1}{m}\sum_{i=1}^{m} y_i^2 - \overline{y}^2}, \quad (6)$$

4.1. Atmosphere—Visual Optic Band

In atmospheric investigations carried out at the IAO SB RAS [13], a copper vapor laser with a wavelength λ = 510.6 nm, pulse repetition frequency around 10–14 kHz, average output power 10–14 W, and pulse duration of 30 ns was used as a source of radiation in the visible range. Pulse-time modulation of the laser beam for information transfer was achieved with a pulse generation control unit [32]. The NLOS communication was realized in the visible range at a wavelength of 510.6 nm for different base distances and weather conditions. Figure 5 shows a map of the experiment carried out in 2016 [13] for a base distance of 69.55 km. A laser beam was distributed over the city of Tomsk, over the Tom' River, a forest between the Tom' and Ob' rivers, and the forests and swamps beyond the Ob' River. The experiment was performed in a cloudless atmosphere with a meteorological visibility range of 15 km. However, it was not possible to implement communication at this baseline distance when, for example, it was raining.

Figure 5. Map illustrating the geometry of our experiment in the visible wavelength range performed in the Tomsk region (Russia).

4.2. Atmosphere—Ultraviolet (UV) Band

In our experiments, a laser at a wavelength of 510.6 nm was used for communication in the atmosphere, and a crystal nonlinearly converted this radiation to wavelengths of 266.3, 272.1, and 289.1 nm, and average power of 0.15–0.5 W. To increase the communication range of bistatic OECS and to decrease the communication errors in our experiments, FF01-442/42-25 (passband 425–470 nm) and LL01-514-12.5 (passband 501.5–526.56 nm) filters were used. Depending on the radiation wavelength, UFK-4G-2 or UFK-4G-4 photomultiplier tubes ("JSC Katod") were included in the receiving system of the OECS. Figure 6a shows a photograph of the placement of a bistatic communication system in a vehicle, and Figure 6b shows the direction of orientation of the optical axis of the receiver with a white arrow. The radiation source is shielded from the receiver by a forest. The basic range was 1.3 km. In Figure 7, the ordinate axis shows the probability of error and its standard deviation (SD), and the abscissa shows the time in relative dimensionless values (to that of free space propagation). We also should note that some works regarding theoretical investigations of NLOS optical systems state that the average power of laser radiation less than 0.5 W is not sufficient for realization of basic ranges of 3 km.

Examples of the probabilistic quality characteristics of the communication channel and images of a sector "mira" recorded in these daytime experiments are shown in Figures 7 and 8 (according to [14]), respectively. Figure 7 illustrates the influence on the communication quality of the weather conditions, which changed during the communication session. It presents the error probabilities (square black symbols) and their standard deviations (vertical lines) on the ordinate axes. Taking into account that a

low-power source of UV radiation (less than 0.5 W) was used in the experiments, it can be assumed that more powerful lasers and more sensitive photo-electronic multipliers will allow long-range UV NLOS systems to reach tens of kilometers.

(**a**) (**b**)

Figure 6. (**a**) Mobile optoelectronic communication systems (OECS); (**b**) direction (white arrow) of the optical axis of the receiving system.

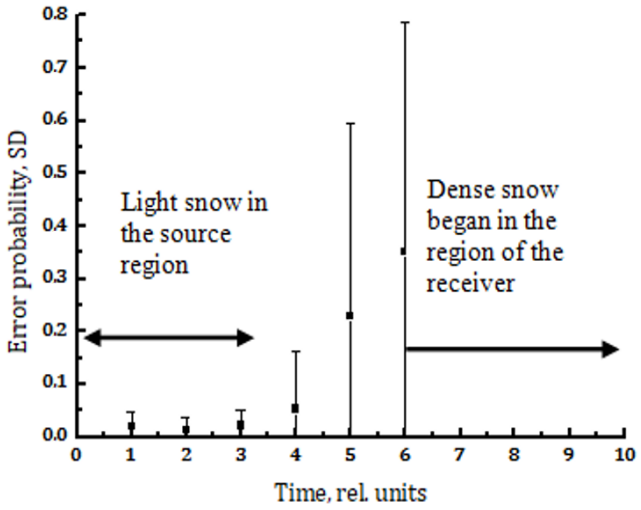

Figure 7. Results of investigation of the communication channel quality in the daytime; external weather conditions—continuous cloudiness.

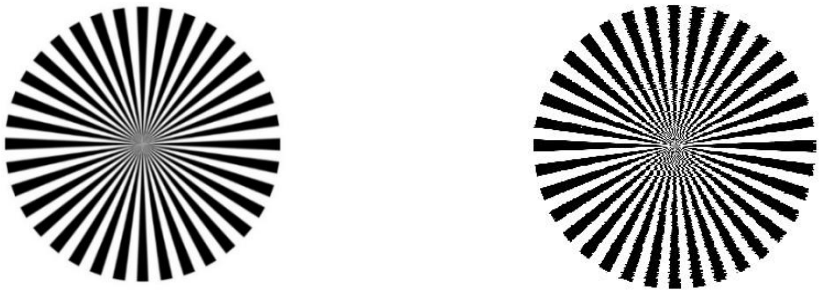

(**a**) (**b**)

Figure 8. (**a**) Examples of the transmitted images; (**b**) received images of a sector "mira" for the same observation conditions as in Figure 7 at time moment 3.

4.3. Underwater Communication

Experimental investigations of underwater communication on scattered or reflected optical radiation have been carried out in the USA, China, Canada, Great Britain, and Russia, amongst others, in both artificial and natural water reservoirs. Discussion of the results of these investigations can be found in [22,24–26]. For example, results of experimental investigations in laboratory conditions were presented in [22] for short communication ranges, not exceeding several meters. Based on the results of these experiments, it was concluded that the range of LOS and of both direct and non-direct NLOS communication systems depends on the water turbidity; as the turbidity increases, the range and maximum data transmission rate decrease. An analytical model of the signal received by the NLOS system was proposed in [26], and results of experiments in a pool were presented for source–receiver distances up to 50 m. Comparison with the theoretical estimates of the signal extinction demonstrated that the proposed model deviated strongly from measurements for base distances around $10 \leq L \leq 50$ m. Over these paths, the signal was attenuated by 6–10 dB, depending on the optical state of the water and the orientation of the source and receiver optical axes. In that work, results were presented of underwater optical communication experiments performed at the Woods Hole Oceanographic Institution, USA, in different reservoirs (from pools to docks) of turbid water at distances up to 40 m.

Important experiments studying underwater bistatic optical communication at the IAO SB RAS were performed in Lake Boyarskoe in the suburb of Tomsk during spring, summer, autumn, and winter, when the ice thickness on its surface reached 50–70 cm. This lake is of the eutrophic trophic type [33], and its maximum depth is 6 m. The average water extinction coefficients were β_{ext} = 1.732–2.108 m^{-1} at the wavelength λ = 510.6 nm, and β_{ext} = 4.169–3.255 m^{-1} at the wavelength λ = 450 nm. Experiments on lakes with open water surfaces were performed in the absence of surface waves. The main goal of the experiments was to determine the maximum achievable baseline distances for the particular NLOS systems.

The radiation sources were: a copper vapor laser with a wavelength of 510.6 nm, average power P = 4–6 W, pulse duration of 30 ns, and pulse repetition frequency 10–14 kHz (a); and a B2000 laser module with a wavelength λ = 450 nm, the same duration and pulse repetition frequency, and average power (after conversion of cw radiation into pulsed radiation) P = 13–20 mW (b). The angular radiation divergence angle did not exceed 1°, and the field-of-view angle of the receiving system was 2°. Geometric schemes illustrating the orientations of the receivers and sources in the experiments are shown in Figure 9.

Experiments with the green laser were performed in February and May 2017, and in February 2019 [34]. The green laser radiation was reflected from mirror No. 1, passed through a hole in the ice, penetrated into the water, and then reflected from mirror No. 2 underwater (see the scheme of the experiment illustrated in Figure 9a). The results were obtained for base distances around $5 \leq L_d \leq 50$ m. Let us consider results of field tests of underwater communication in summer. One of the primary goals of these experiments was to determine the maximal base distance L_d for fixed characteristics and parameters of the source and receiver systems. In our experiments, the angle α was fixed for each L_d value, and the angle β was varied (Figure 9b). The probabilities and SD of communication errors were estimated in real time. From 7000 to 90,000 symbols were transmitted during each communication session that lasted from 7 to 30 min. Each experiment lasted from 1 to 3 h. The base distance L_d increased in steps of 5 m, starting from 5 m. The maximal base distance was 40 m, which was in complete agreement with the results obtained in a pool reported in [34]. Results of experiments performed in winter were close to summer data. The maximal base distance reached 40 m for the green information-bearing laser beam (λ = 510.6 nm, P = 4–6 W) and 20 m for the dark blue laser source (λ = 450 nm, P = 13–20 mW). Figure 10 illustrates the scheme of experiments in water under the ice surface (top view) performed in Lake Boyarskoe in winter 2019 with the green laser.

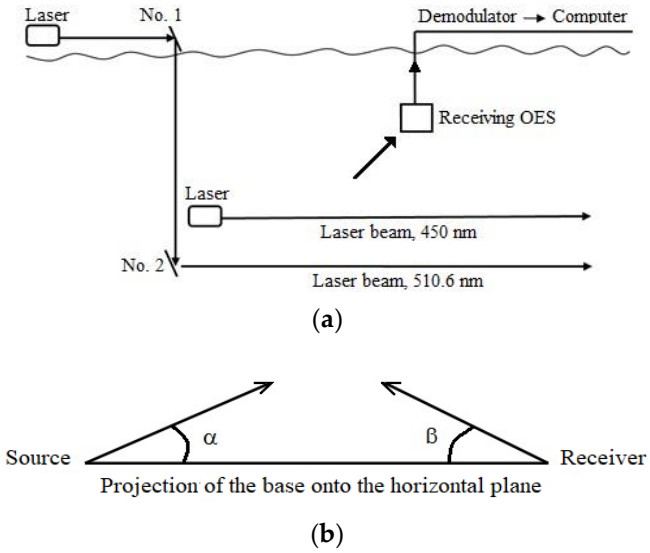

Figure 9. Geometric schemes of experiments: (**a**) side view: the green laser is placed on the bank of the lake, and the dark blue laser is immersed in water; (**b**) top view: directions of the optical axes of the source and receiving systems.

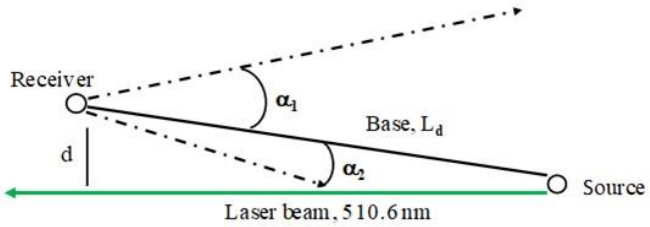

Figure 10. Geometric scheme of experiments (2019) in water under the ice surface described by Figure 9a.

In these experiments, the base distances L_d, angles α_1 and α_2, and distances d were varied. The angles α_1 and α_2 are measured from the base distances L_d (the solid black curve in the figure) to the optical axis of the receiving system (dash-dotted curve). They varied between $45° > \alpha_1 > 0°$ and $45° > \alpha_2 > 0°$. An analysis of the dependence of the estimated error probabilities and SD on these parameters led to the following conclusion. When $d \to 0$, the probabilities of errors and their SD decreased. This is caused by the fact that at fixed α_1 and α_2, and when $d \to 0$, the receiver records the intensity of radiation scattered at angles approaching 0°. The probabilities of errors and SD decreased for the same reasons when α_1 (or α_2) $\to 0$ (Figure 11). In Figure 11, the ordinate axis shows the probability of error and its standard deviation (SD), and the abscissa shows time in relative dimensionless values (to that of free space propagation). Figure 12 shows a photograph of the laser beam propagating at a distance of 1 m from the lower ice boundary. The distance between the source and the camera was 15 m, and the camera was placed at a distance d = 3 m (Figure 10, $\alpha_2 = 30°$).

As expected, the transmission range of bistatic underwater optical communication systems depended significantly on the water turbidity. For example, in experiments near Lake Rozhnevo (Tomsk region), the maximal range L_d was less than 1.5 m at λ = 450 nm and P = 13–20 mW, while in Lake Boyarskoe, L_d reached 20 m. This is explained by the fact that the water extinction coefficient near Rozhnevo Island was β_{ext} = 31.130 m^{-1}, whereas for the water of Lake Boyarskoe, β_{ext} = 4.107 m^{-1}. We emphasize that the water extinction coefficient of Lake Rozhnevo was considerably higher than that of the water in Lake Boyarskoe, due to significantly higher absorption. We note that even in the absence of the external factors influencing the optical properties of water (water was screened

from the atmosphere, there were no streams), the average probabilities of communication errors and their SD depended on the time of information recording. This can be explained by the presence in water of moving small-size organisms, as demonstrated in our observations using a high-sensitivity video camera.

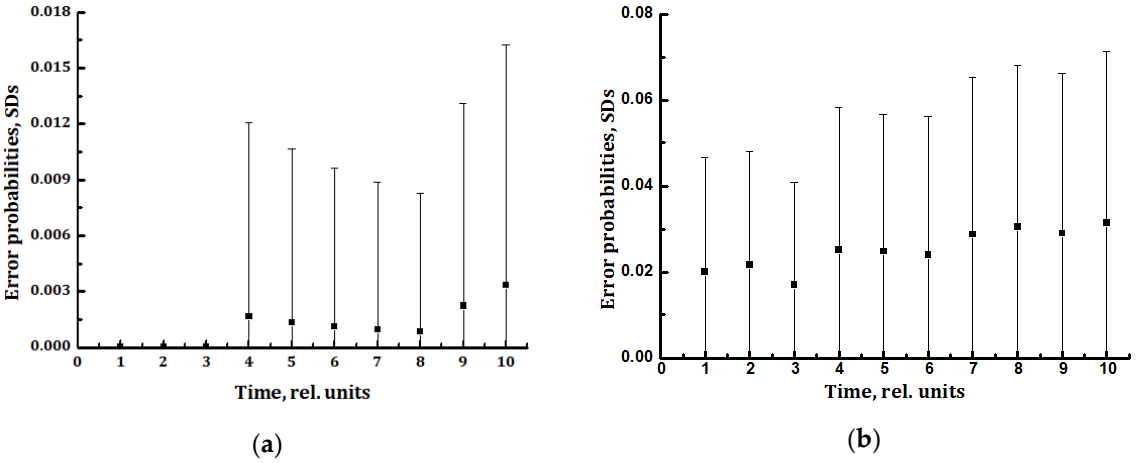

Figure 11. Examples of the estimated probabilities of error and SD for underwater communication experiments beneath the ice surface using the scheme shown in Figure 10: (**a**) with $\alpha_2 = 30°$; (**b**) $\alpha_1 = 30°$.

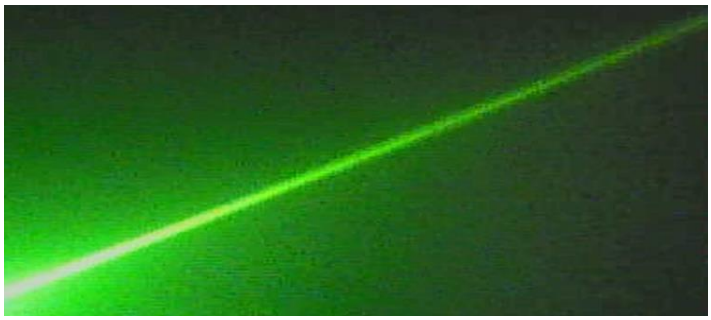

Figure 12. Photograph of a laser beam under the ice surface: side view.

5. Conclusions

In recent decades, comprehensive theoretical and experimental investigations of optical communication systems based on scattered laser radiation have been carried out in atmospheric and water media in Russia. Results of these investigations have been published in [7,9,13,14,19,20,34]. Theoretical research has been carried out using the Monte Carlo method. For this purpose, a new modification of the algorithm of double local estimate has been developed for the purpose of simulation of the impulse response of external (atmospheric or water) channels with optical radiation scattering and absorption [7]. Simulations have been carried out in a wide range of optical-geometric conditions of observations, and employing coplanar NLOS communication schemes [9]. Atmospheric NLOS communication systems with radiation sources in the visible, near-IR, and UV wavelength ranges (λ = 300, 500, and 900 nm) for meteorological visibility between 10 and 50 km have been investigated. Underwater NLOS communication systems have been considered for radiation sources at a wavelength of 300 nm and visibility depth of 30 m for a wide range of orientation angles of the source and receiver optical axes [20].

A new effective version of the Monte Carlo double local estimation algorithm has been created for the statistical simulation of the impulse response characteristics of coplanar atmospheric and underwater NLOS channels taking into account multiple scattering and absorption of optical radiation in dispersed media. Monte Carlo simulations have been used to estimate the maximum transmission ranges and the

pulse transfer characteristics for these hypothetical communication systems, taking into account the parameters of photoelectron multipliers [9,20]. In particular, for atmospheric communication systems, the conditions under which these ranges can reach more than 100 km with a pulse transfer rate of 2×10^7 Hz have been determined. Underwater NLOS communication was realized for base distances around 10–100 m and pulse transfer rates from 3×10^6 Hz to 2×10^7 Hz. Based on numerical experiments, for the first time, the limiting ranges of action and transmission rates of pulses in bistatic communication systems were established for radiation sources at wavelengths of 300, 500, and 900 nm for given angles of divergence of radiation, field of view of receivers, and meteorological ranges of visibility in the atmosphere. Scanning the corresponding global literature regarding similar investigations allows us to emphasize that there are no analogues in studies of competing scientific groups.

Experimental investigations of atmospheric and underwater NLOS communication systems were performed outdoors in Russia. No laboratory experiments were carried out for these purposes. For the first time, a method for estimating the probabilities of communication errors and their standard deviations in real time has been proposed and implemented. It can be used to diagnose the quality of NLOS communication channels and select the characteristics of the transmitter–receiver units to ensure their maximum quality. To evaluate the performance of NLOS communication in real time, a simple technique of estimating the communication error probabilities and SD was used in the experiments.

NLOS communication was realized for base distances up to 70 km in the visible range at a wavelength of 510.6 nm at night, and up to 1.3 km in the UV range at a wavelength of 255.3 nm in the daytime and at night. The experiments were performed under different meteorological conditions in the atmosphere, which varied during the experiments. Underwater NLOS communication was carried out in a freshwater lake (including under ice) at radiation wavelengths of 510.6 and 450 nm at basic distances of up to 40 m. In the forefront of the experimental investigations carried out in Russia stand the underwater NLOS communication trials, including communication under ice. This communication was realized with sources in the visible range, at wavelengths of 510.6 and 450 nm and at distances up to 40 m. We emphasize no data exist in the literature on NLOS experiments of other scientific groups carried out under ice.

In our future research, we plan to conduct NLOS experiments in the IR range at a wavelength of 1064 nm together with our co-authors, commencing in the middle of 2021.

Funding: This research received no external funding.

Acknowledgments: The authors wish to thank G.G. Matvienko and I.V. Ptashnik, directors of the V.E. Zuev Institute of Atmospheric Optics of the Siberian Branch of the Russian Academy of Science.

Conflicts of Interest: The authors declare that there are no conflict of interest related to this article.

References

1. Kaushall, H.; Kaddoum, G. Underwater optical wireless communication. *IEEE Access* **2016**, *4*, 1518–1547. [CrossRef]
2. Poller, B.V. Wireless local optical networks with possibilities of application of an atmospheric communication channel with scattering. In Proceedings of the Collection of Reports Presented at the 10th Int. Sci.-Tech. Conf. Radar Detection and Ranging, Navigation, and Communication, Voronezh, Russia, 3–15 April 2004; pp. 1265–1270.
3. Kopeika, N.S.; Bordogna, J. Background noise in optical communication systems. *Proc. IEEE* **1970**, *58*, 1571–1577. [CrossRef]
4. Blaunstein, N.; Kopeika, N. (Eds.) *Optical Waves and Laser Beams in the Irregular Atmosphere*; CRC Press: Boca Raton, FL, USA, 2018.
5. Kedar, D. Multiaccess interference in a non-line-of-sight ultraviolet optical wireless sensor network. *Appl. Opt.* **2007**, *46*, 5895–5901. [CrossRef] [PubMed]
6. Ding, H.; Chen, G.; Majumdar, A.K.; Sadler, B.M.; Xu, Z. Modeling of non-line-of-sight ultraviolet scattering channels for communication. *IEEE J. Sel. Areas Commun.* **2009**, *27*, 1535–1541. [CrossRef]

7. Belov, V.V.; Tarasenkov, M.V. Three algorithms of statistical modeling in problems of optical communication on scattered radiation and bistatic sensing. *Atmos. Ocean. Opt.* **2016**, *29*, 533–540. [CrossRef]
8. Chvojka, P.; Vitek, S.; Zvanovec, S.; Ghassemlooy, Z.; Rajbhandari, S. Analysis of non-line-of-sight visible light communications. *Opt. Eng.* **2017**, *56*, 116116. [CrossRef]
9. Tarasenkov, M.V.; Poznaharev, E.S.; Belov, V.V. Statistical estimates of transfer characteristics, maximal ranges, and rates of information transfer through pulsed atmospheric bistatic optical communication channels. *Svetotekhnika (Light Tech.)* **2018**, *4*, 37–43.
10. Drost, R.J.; Moore, T.J.; Sadler, B.M. Ultraviolet scattering propagation modeling: Analysis of path loss versus range. *J. Opt. Soc. Am. A* **2013**, *30*, 2259–2265. [CrossRef]
11. Bifeng, L.; Hongxing, W.; Min, L.; Hao, H.; Zhongyang, M. Applicability of non-line-of-sight ultraviolet single-scatter approximation model. *Photon. Netw. Commun.* **2016**, *31*, 147–154.
12. Juwiler, I.; Bronfman, I.; Blaunstein, N. Analysis of total signal decay and capacity of information data in wireless atmospheric communication links. Part 1. *Inf. Control Syst.* **2019**, *98*, 43–53. [CrossRef]
13. Abramochkin, V.N.; Belov, V.V.; Gridnev, Y.V.; Kudryavtsev, A.N.; Tarasenkov, M.V.; Fedosov, A.V. Optoelectronic communication in the atmosphere using diffuse laser radiation: Experiments in the field. *Light Eng.* **2017**, *25*, 41–49.
14. Belov, V.V.; Gridnev, Y.V.; Kudryavtsev, A.N.; Tarasenkov, M.V.; Fedosov, A.V. Optoelectronic UV communication on scattered laser radiation. *Atmos. Ocean. Opt.* **2018**, *31*, 698–701. [CrossRef]
15. Menglong, W.; Dahai, H.; Xiang, Z.; Feng, Z.; Min, Z.; Guangxin, Y. Experimental research and comparison of LDPC and RS channel coding in ultraviolet communication systems. *Opt. Express* **2014**, *22*, 5422–5430.
16. Shaw, G.A.; Siegel, A.M.; Nischan, M.L. Demonstration system and applications for compact wireless ultraviolet communications. *Proc. SPIE* **2003**, *5071*. [CrossRef]
17. Chen, G.; Xu, Z.; Sadler, B.M. Experimental demonstration of ultraviolet pulse broadening in short-range non-line-of-sight communication channels. *Opt. Express* **2010**, *18*, 10500–10509. [CrossRef] [PubMed]
18. Dahai, H.; Yile, L.; Kai, Z.; Pengfei, L.; Min, Z. Theoretical and experimental research on diversity reception technology in NLOS UV communication system. *Opt. Express* **2012**, *20*, 15833–15843.
19. Belov, V.V. Optical communication on scattered laser radiation. *Proc. SPIE* **2017**, *10466*, 104660H.
20. Tarasenkov, M.V.; Belov, V.V.; Poznakharev, E.S. Statistical simulation of the characteristics of diffuse underwater optical communication. *Atmos. Ocean. Opt.* **2019**, *32*, 387–392. [CrossRef]
21. Chadi, G.; Khalighi, M.-A.; Salah, B.; Pierre, L.; Rigaud, V. Monte-Carlo-Based channel characterization for underwater optical communication systems. *IEEE/OSA J. Opt. Commun. Netw.* **2013**, *5*, 1–12.
22. Choudhary, A.; Jagadeesh, V.K.; Muthuchidambaranathan, P. Pathloss analysis of NLOS underwater wireless optical communication channel. In Proceedings of the International Conference on Electronics and Communication System (ICECS-2014), Coimbatore, India, 13–14 February 2014; pp. 1–6.
23. Hanson, F.; Radic, S. High bandwidth underwater optical communication. *Appl. Opt.* **2008**, *47*, 277–283. [CrossRef]
24. Arnon, S.; Kedar, D. Non-line-of-sight underwater optical wireless communication network. *J. Opt. Soc. Am. A* **2009**, *26*, 530–539. [CrossRef] [PubMed]
25. Doniec, M.; Angermann, M.; Rus, D. An end-to-end signal strength model for underwater optical communications. *Browse J. Magazines IEEE J. Ocean. Eng.* **2013**, *38*, 743–757. [CrossRef]
26. Blaunstein, N.; Arnon, S.; Kopeika, N.; Zilberman, A. *Applied Aspects of Optical Communication and Lidar*; CRC Press: Boca Raton, FL, USA, 2010.
27. Zuev, V.E.; Krekov, G.M. *Current Problems of Atmospheric Optics, Volume 2: Optical Models of the Atmosphere*; Gidrometeoizdat: Leningrad, Russia, 1986.
28. Zuev, V.E.; Belan, B.D.; Zadde, G.O. *Optical Weather*; Nauka: Novosibirsk, Russia, 1990.
29. Shifrin, K.S. (Ed.) *Ocean and Atmospheric Optics*; Nauka: Moscow, Russia, 1981.
30. Monin, A.S. (Ed.) *Ocean Optics, Vol. 2: Applied Ocean Optics*; Nauka: Moscow, Russia, 1983.
31. Monin, A.S. (Ed.) *Ocean Optics, Vol. 1: Physical Ocean Optics*; Nauka: Moscow, Russia, 1983.
32. Dimaki, V.A.; Sukhanov, V.B.; Troitskii, V.O.; Filonov, A.G.; Shestakov, D.Y. Computer-controlled bromide copper vapor laser of pulsed-periodic, pulse train, and waiting operation modes. *J. Devices Tech. Exp. (Pribory Tekhnika Eksperimenta)* **2008**, *6*, 119–122.

33. Sutorikhin, I.A.; Bukatyi, V.I.; Akulova, O.B. *Spectral Transparency of Water in Polytypic Lakes of Altay Territory*; Publishing House of Altai State University: Barnaul, Russia, 2015.
34. Belov, V.V.; Abramochkin, V.N.; Gridnev, Y.V.; Kudryavtsev, A.N.; Tarasenkov, M.V.; Fedosov, A.V.; Poznakharev, E.S. Experimental and theoretical investigations in the SB RAS on problems of bistatic underwater optical communication. *Proc. SPIE* **2019**, *11208*. [CrossRef]